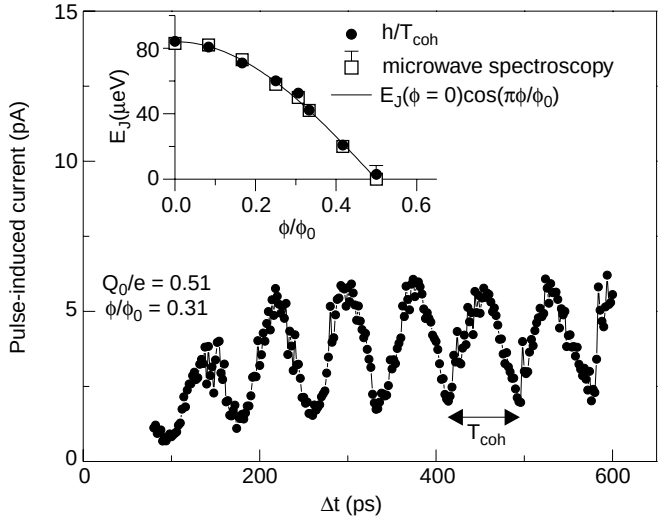

Figure 4 Pulse-induced current as a function of the pulse length Δt. The data correspond to the cross-section of Fig. 3a at $Q_0/e = 0.51$. Inset, Josephson energy E_J versus the magnetic flux ϕ penetrating through the loop. E_J was estimated by two independent methods. One was from the period of the coherent oscillation T_{coh} as h/T_{coh}. The other was from the gap energy observed in microwave spectroscopy[4]. The solid line shows a fitting curve with $E_J(\phi = 0) = 84\,\mu$eV assuming cosine ϕ-dependence of E_J.

Figure 4 shows the pulse-induced current at $Q_0/e = 0.51$ as a function of Δt, showing that the coherent oscillation can be observed in the time domain and that we can control the quantum state through an arbitrary pulse length Δt. The oscillation amplitude was smaller than that simply expected from $2e$ per pulse, $2e/T_r = 20$ pA. The finite rise and fall times of the pulse might explain this deviation. We recall that in the limit of long rise and fall times (the adiabatic limit), there would be no transition probability to $|2\rangle$. For the realistic rise and fall times of the pulse we assumed in the simulation above, for example, the amplitude of the oscillations in $\langle\Delta P(2)\rangle$ at $Q_0/e = 0.51$ is reduced to ~0.4, by which the current signal would be decreased. Moreover, the finite repetition time (not much longer than $\Gamma_{qp1}^{-1} + \Gamma_{qp2}^{-1}$) could also reduce the signal due to the incomplete relaxation of $|2\rangle$ to $|0\rangle$ after each pulse.

To further confirm that the observed oscillation was coherent oscillation due to Josephson coupling, we estimated the Josephson energy E_J from the oscillation period T_{coh} as $E_J = h/T_{coh}$ and investigated its magnetic-field dependence (filled circles in Fig. 4 inset). We also measured E_J in the frequency domain through microwave spectroscopy of the energy-level splitting[4] (open squares in Fig. 4 inset). The two sets of data agreed very well, and fitted the expected cosine curve.

For future application as quantum computing devices[5–7], a crucial parameter is the decoherence time. The main decoherence source in a single-Cooper-pair box is thought to be spontaneous photon emission to the electromagnetic environment[1,5–7], and the decoherence time could exceed 1 μs. But when a probe junction is used, as in our set-up, the 'detection' with quasiparticle tunnelling through the probe junction would be the main source of decoherence. So far, we have observed oscillation up to $\Delta t \approx 2$ ns, although low-frequency background-charge fluctuation degraded the direct current signal and made it difficult to determine the envelope of the decay. A more detailed study of the decoherence time would provide important information for designing solid-state quantum circuits using superconducting single-Cooper-pair boxes. □

Received 26 January; accepted 18 March 1999.

1. Bouchiat, V., Vion, D., Joyez, P., Esteve, D. & Devoret, M. H. Quantum coherence with a single Cooper pair. *Physica Scripta T* **76,** 165–170 (1998).
2. Joyez, P., Lafarge, P., Filipe, A., Esteve, D. & Devoret, M. H. Observation of parity-induced suppression of Josephson tunneling in the superconducting single electron transistor. *Phys. Rev. Lett.* **72,** 2458–2461 (1994).
3. Flees, D., Han, S. & Lukens, J. Interband transitions and band gap measurements in Bloch transistors. *Phys. Rev. Lett.* **78,** 4817–4820 (1997).
4. Nakamura, Y., Chen, C. D. & Tsai, J. S. Spectroscopy of energy-level splitting between two macroscopic quantum states of charge coherently superposed by Josephson coupling. *Phys. Rev. Lett.* **79,** 2328–2331 (1997).
5. Shnirman, A., Schön, G. & Hermon, Z. Quantum manipulation of small Josephson junctions. *Phys. Rev. Lett.* **79,** 2371–2374 (1997).
6. Averin, D. V. Adiabatic quantum computation with Cooper pairs. *Solid State Commun.* **105,** 659–664 (1998).
7. Makhlin, Yu., Schön, G. & Shnirman, A. Josephson-junction qubits with controlled couplings. *Nature* **398,** 305–307 (1999).
8. Shedelbeck, G., Wegscheider, W., Bichler, M. & Abstreiter, G. Coupled quantum dots fabricated by cleaved edge overgrowth: from artificial atoms to molecules. *Science* **278,** 1792–1795 (1997).
9. Oosterkamp, T. H. *et al.* Microwave spectroscopy of a quantum-dot molecule. *Nature* **395,** 873–876 (1998).
10. Bonadeo, N. H. *et al.* Coherent optical control of the quantum state of a single quantum dot. *Science* **282,** 1473–1476 (1998).
11. Loss, D. & DiVincenzo, D. P. Quantum computation with quantum dots. *Phys. Rev. A* **57,** 120–126 (1998).
12. Kane, B. E. A silicon-based nuclear spin quantum computer. *Nature* **393,** 133–137 (1998).
13. Leggett, A. J. in *Chance and Matter* (eds Souletie, J., Vannimenus, J. & Stora, R.) 395–506 (Elsevier, Amsterdam, 1984).
14. Tesche, C. D. Can a noninvasive measurement of magnetic flux be performed with superconducting circuits? *Phys. Rev. Lett.* **64,** 2358–2361 (1990).
15. Neumann, F., Ingold, G.-L. & Grabert, H. Influence of the environment on charge quantization in small superconducting islands. *Phys. Rev. B* **50,** 12811–12819 (1994).
16. Fulton, T. A., Gammel, P. L., Bishop, D. J., Dunkleberger, L. N. & Dolan, G. J. Observation of combined Josephson and charging effects in small tunnel junction circuits. *Phys. Rev. Lett.* **63,** 1307–1310 (1989).
17. Averin, D. V. & Aleshkin, V. Ya. Resonant tunneling of Cooper pairs in a system of two small Josephson junctions. *JETP Lett.* **50,** 367–369 (1989).

Acknowledgements. We thank W. Hattori, M. Baba and H. Suzuki for experimental help and M. Ueda, Y. Kohno, M. H. Devoret and Y. Ootuka for discussions. This work was supported by the Core Research for Evolutional Science and Technology (CREST) of the Japan Science and Technology Corporation (JST).

Correspondence and requests for materials should be addressed to Y.N. (e-mail: yasunobu@frl.cl.nec.co.jp).

The existence of supercooled liquid water at 150 K

R. Scott Smith & Bruce D. Kay

Environmental Molecular Sciences Laboratory, Pacific Northwest National Laboratory, PO Box 999, Mail Stop K8-88, Richland, Washington 99352, USA

Supercooled water may offer clues to the anomalous properties of its normal liquid state[1]. The supercooled state also shows anomalous thermodynamic and transport properties at low temperatures[2–4]. Although there are several theoretical explanations for this behaviour, no consensus has emerged[1,2,5–12]. Some theories preclude the existence of the supercooled liquid below an apparent thermodynamic singularity at 228 K (refs 2, 7, 9); others are consistent with a continuous region of metastability from the melting point at 273 K to the glass transition temperature at 136 K (refs 6, 8, 13). But the data needed to distinguish between these possibilities have not yet been forthcoming. Here we determine the diffusivity of amorphous ice by studying isotope intermixing in films less than 500 nanometres thick. The magnitude and temperature dependence of the diffusivity is consistent with the idea that the amorphous solid water melts into a deeply metastable extension of normal liquid water before crystallizing at 160 K. This argues against the idea of a singularity in the supercooled regime at ambient pressure.

Water vapour deposited on low-temperature substrates (<140 K) is known to form an amorphous phase, termed amorphous solid water (ASW), that is metastable with respect to crystalline ice[3,4,14]. There is still a debate about whether this amorphous form of water transforms to a metastable liquid above the glass transition temperature at 136 K and before crystallization near 160 K (refs 15–17). Furthermore, if the amorphous solid does melt into a liquid, a question remains as to whether this liquid is a metastable extension of supercooled liquid water or a distinct thermodynamic phase[15–17]. We have recently measured the difference in the vapour pressure

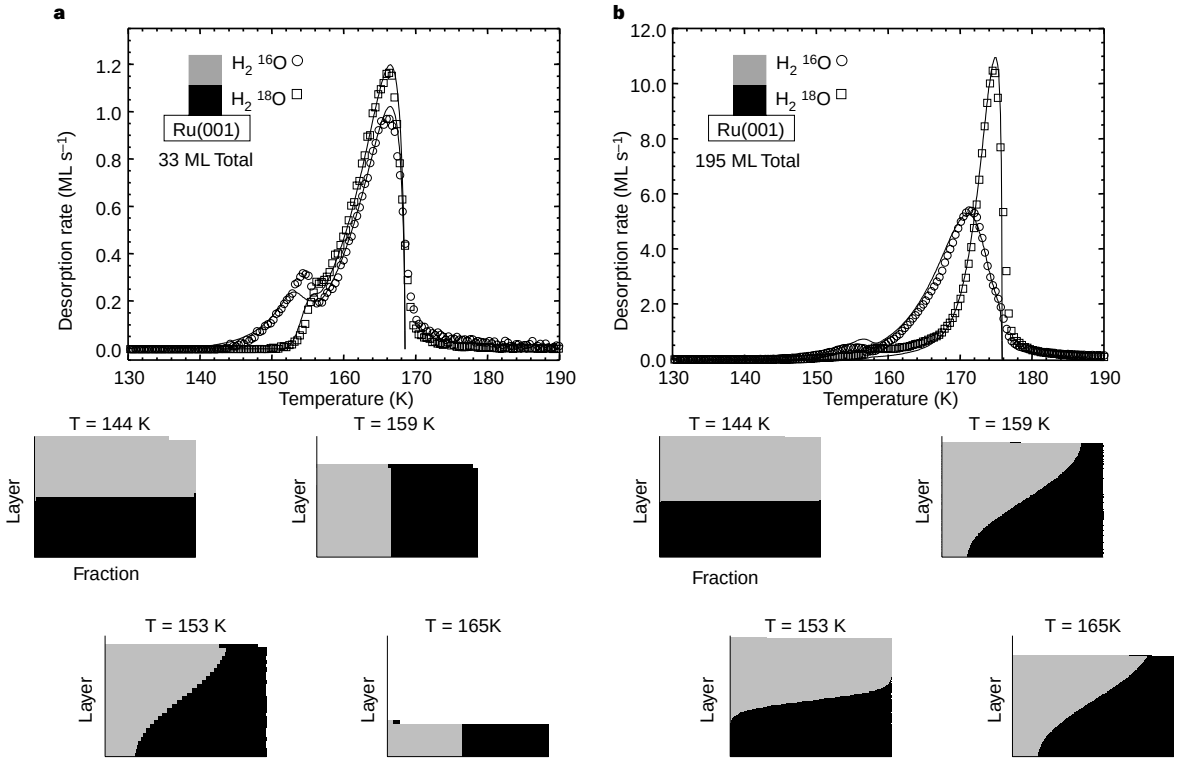

Figure 1 Comparison of TPD experiment and model simulation. The nanoscale films were created using an effusive molecular beam having a flux of ~0.06 monolayers per second, ML s^{-1} (1 ML = ~10^{15} molecules cm^{-2}). Water deposits were made at 85 K, and the temperature was then linearly ramped at a rate of 0.6 K s^{-1}. **a**, The TPD spectra (top) for an experiment where ~17 layers of $H_2{}^{16}O$ (open circles) were deposited on ~16 layers of $H_2{}^{18}O$ (open squares); the model simulation (solid line) is also shown. The experiments and simulation are in excellent agreement. The desorption data show that below 154 K only $H_2{}^{16}O$ (the species on top) desorbs, but after the phase transition the desorption rates are nearly equal which indicates significant mixing. Bottom, the graphs below the TPD spectra are concentration profiles that reveal the layer-by-layer extent of mixing of the two isotopes at the given temperature. The mole fraction of each isotopic species ($H_2{}^{16}O$ (light shade) and $H_2{}^{18}O$ (dark shade)) within a given layer is represented as a horizontal bar graph. The profile at 144 K shows that the isotopes have not mixed, as the top layers consist of only the $H_2{}^{16}O$ isotope while the bottom layers consist of only the $H_2{}^{18}O$ isotope. But by 159 K the two isotopes have completely mixed, as is shown by the nearly equal amounts of the two isotopes in each layer. At higher temperatures the thin film has crystallized, so diffusion is 'frozen' and the concentration profile remains constant as the water film desorbs. **b**, The TPD spectra (top) for an experiment where ~100 layers of $H_2{}^{16}O$ (open circles) were deposited on ~95 layers of $H_2{}^{18}O$ (open squares) to create a 195-ML-thick film; the model simulation (solid line) is also shown. The desorption data show that a large fraction of the $H_2{}^{16}O$ (species on top) desorbs before the onset of significant $H_2{}^{18}O$ (species on bottom) desorption. The concentration profiles (bottom) show that although at 153 K the films have begun to mix, at 159 K the two isotopes have not completely mixed before crystallization of the thin film. The distribution is effectively "frozen" by the complete crystallization above 159 K. The use of thin water isotopic films to determine the extent of intermixing has been demonstrated previously[18]. The growth conditions used here produce optically flat non-porous water films[19,37]. A roughened interface between the isotopic layers, which in the worst case would result in intermixing of $\sqrt{N}$ (where N is the number of layers), cannot account for the observed intermixing. The possibility of crack formation during the crystallization has also been studied[21]. Our kinetic model would not be able to reproduce the experimental data if the dominant intermixing mechanism were mixing along (or through) cracks formed in the films. Furthermore, such a mechanism could not account for the statistical isotopic exchange product yields shown previously[18].

between ASW and crystalline ice and determined that thermodynamic continuity with normal liquid water is possible[17]. We have also shown that long-range molecular translational diffusion characteristic of liquid-like behaviour occurs before crystallization[18]. Estimates of the liquid diffusion coefficients yield a diffusivity roughly a million times greater than that of crystalline ice[18].

We employ molecular beams of $H_2{}^{16}O$ and $H_2{}^{18}O$ with high spatial resolution to create nanoscale ASW films (<5,000 Å thick). Temperature-programmed desorption (TPD) is used to measure quantitatively the desorption kinetics, and thereby reveal the extent of mixing between the $H_2{}^{16}O$ and $H_2{}^{18}O$ layered interfaces[17–21]. Quantitative measurements of the desorption rates from the amorphous and crystalline phases of H_2O and D_2O have been used to quantify the crystallization kinetics which can be described by a classic nucleation and growth mechanism[17,20]. The conversion to the thermodynamically stable crystalline phase results in a concomitant decrease in the vapour pressure (desorption rate) and the irreversible amorphous to crystalline transformation[14,18,20,21] appears as a 'bump' in the 150–160 K temperature range of the TPD spectrum.

We quantify the temperature-dependent diffusivity using a mathematical model that couples our previous mean-field description of the desorption/crystallization kinetics[20] to a one-dimensional representation of the diffusive transport between layers. The effective diffusivity is a linear combination of the amorphous and crystalline diffusion coefficients weighted by their respective mole fractions. We assume an Arrhenius form for the temperature dependence of the diffusion coefficients, and vary the amorphous diffusion parameters to achieve a fit to the experimental data.

Figure 1 shows TPD spectra and model simulations for two different total thicknesses of ASW. As shown in Fig. 1a, the onset of isotopic mixing is abrupt and is concomitant with the phase transformation of ASW into crystalline ice. If the isotopically tailored layers did not exhibit diffusive intermixing, all of the $H_2{}^{16}O$ molecules would desorb before the onset of $H_2{}^{18}O$ desorption. This would be expected if the ASW phase had the diffusivity of

crystalline ice. The simulation results (solid lines) are in excellent agreement with the experiment. The four illustrations in the bottom of Fig. 1a show the vertical spatial distribution of the isotopes obtained from the simulation. At 144 K the two isotopes are vertically separated as deposited, but by 153 K significant intermixing has occurred. At 159 K the layers have completely mixed and the film has crystallized.

Figure 1b shows the experimental TPD spectra and the model simulation for a much thicker film. These spectra reveal that only a limited amount of mixing has occurred before complete crystallization. The vertical spatial distributions of the isotopes, illustrated in the bottom of the figure, show that mixing occurs in concert with the phase transition but that at 159 K the film has not mixed completely. Above 159 K the film is completely crystallized, and as such, the diffusive motion is 'frozen out'. As the film thickness increases, the films show departures from complete mixing because the effective mixing zone is limited by the time it takes for the film to crystallize. We have performed similar experiments for a variety of films, and find that the model simulation with a single set of amorphous diffusion parameters is in excellent agreement with the experimental data for thicknesses from 30 to 200 monolayers (ML) irrespective of which isotope is on top. Although not shown here, experiments using H/D labelled water reveal complete isotopic scrambling within the intermixed region, thereby demonstrating intimate chemical contact between the species[18].

The temperature dependence of the diffusivity obtained from the simulation is shown in Fig. 2. In Fig. 2a the diffusivity (solid line) shows an initial exponential rise with temperature but reaches a maximum near 157 K and then drops rapidly. As the fraction crystallized[17,18,20,21] increases from 0 to 1 (dashed line), the diffusivity transforms from completely amorphous diffusion to completely crystalline diffusion. As the diffusion in the amorphous liquid phase is much easier than in the crystalline solid phase, the effective diffusivity shows a maximum when plotted as a function of temperature. The diffusivity is shown in an Arrhenius plot in Fig. 2b. The low-temperature diffusivity data show that the amorphous diffusion has a relatively high activation energy. An Arrhenius fit (dashed line) to the diffusivity over the temperature range 147–157 K yields an apparent activation energy of 170 ± 40 kJ. The large uncertainty in the activation energy is due to the insensitivity of the simulations to the slope of the Arrhenius fit over the narrow temperature range before the onset of crystallization. Nonetheless, the simulations are extremely sensitive to ±50% variations in the absolute value of the amorphous diffusivity over this narrow temperature range. Above 157 K, the diffusivity drops rapidly owing to crystallization. Diffusion in crystalline ice in this temperature range (up to 170 K) is extremely small[22,23], and nearly identical simulation results are obtained when the value of crystalline diffusion is set to zero. Near 160 K the diffusivity of ASW reaches $\sim 10^{-12}$ cm^2 s^{-1}, roughly 10^7 times smaller than the diffusivity of normal liquid water at room temperature. Such a diffusivity would be nearly impossible to observe with a macroscopic sample—a 1-cm-thick film would require $\sim 10^5$ years to mix completely. The use of nanoscale films enables these small diffusivities to be determined quantitatively.

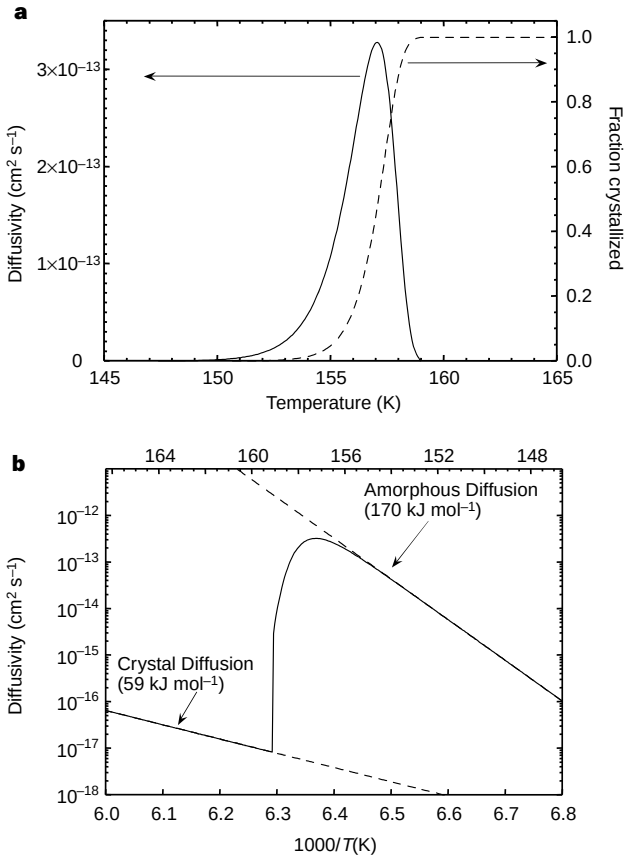

Figure 2 Diffusivity versus temperature from the model simulation of the TPD experimental data. **a**, The solid line is the diffusivity versus temperature, and the dashed line is the extent of crystallization of the ASW material. The maximum in the plot of diffusivity versus temperature is because the diffusivity in the amorphous liquid phase is much greater than that in the crystalline solid phase. **b**, An Arrhenius plot of the same diffusivity data (solid line). The dashed lines are Arrhenius fits to the pure amorphous and pure crystalline diffusion regions. The apparent activation energies for amorphous and crystalline diffusion are 170 and 59 kJ mol^{-1}, respectively.

Figure 3 shows the temperature dependence of the diffusivity for ASW, liquid water[24], supercooled liquid water[25,26], and crystalline ice[22,23]. An Arrhenius extrapolation of the liquid and supercooled liquid data does not agree with our ASW diffusivity results; our results show a much stronger temperature dependence, with an apparent activation energy of ~170 kJ mol^{-1}. It is known that glass-forming liquids show markedly non-Arrhenius behaviour as they are supercooled below their freezing point[5,27]. The temperature dependence of this non-Arrhenius behaviour is often well represented by the empirical Vogel–Fulcher–Tammann (VFT) equation[5,27], $D = D_o \exp - [E/(T - T_o)]$ where D is the temperature dependent diffusivity, T is the temperature, and D_0, E and T_0 are fit parameters. The solid line labelled VFT in Fig. 3 is the result of fitting all of the diffusivity data to the VFT equation.

It has been proposed[2] that there is a thermodynamic singularity in the water phase diagram at 228 K. This proposal was partly based on the observation that many of the physical properties of supercooled water could be described by a power-law equation of the form, $A = A_o(T/T_s - 1)^\gamma$, where A is the property of interest and A_o, γ and T_s are fit parameters. One interpretation of this singularity is given by the "stability limit conjecture", which predicts that normal liquid water cannot exist below T_s, due to a retracing spinodal[7]. Another interpretation is that the apparent singularity is due to the existence of a second critical point in the water phase diagram[8,12]. The power-law prediction for the liquid and supercooled-liquid diffusivity data is plotted in Fig. 3. Over the temperature range 250–500 K, a comparison of the fits does not provide unambiguous evidence in support of either the VFT or power-law equations. On an expanded scale (Fig. 3 inset), the VFT equation deviates from the liquid data below 250 K by about 25% and the power law gives a better fit. However, assuming that the diffusivities from the two temperature regions can be connected, then the VFT equation describes the entire set of data spanning a range of 10^{10} reasonably well (within a ±25% deviation). We note that the power-law equation, or any equation with a temperature singularity at 228 K, cannot fit both the ASW and the liquid diffusivity data.

The open question is whether there is a continuity between the normal supercooled-liquid diffusivity and the liquid-like diffusivity

near 150 K. The ASW diffusivity data provide for an interpretation that does not require either a singularity at 228 K (refs 3, 28, 29) or a new distinct phase of liquid water[16,17]. The continuity interpretation is supported by additional experimental evidence. The markedly non-Arrhenius behaviour of the VFT fit is consistent with that of a fragile liquid[5,27] having an ideal glass transition temperature, $T_o = 118$ K (ref. 4). This value is consistent with the experimental calorimetric glass transition temperature, T_g, observed between 124 and 136 K (refs 30, 31). The rapid decrease in diffusivity on cooling towards the glass temperature is also consistent with the observation of no translational diffusion at 125 K within 13.5 hours (ref. 15). Recent mechanical deformation studies support the liquid-like behaviour of ASW above its T_g (ref. 32). Furthermore, recent low-temperature measurements (163–174 K) indicate that the dielectric relaxation of water has a VFT-like temperature dependence, similar to that shown in Fig. 3 for the self-diffusivity[32,33]. Further evidence against a low-pressure singularity at 228 K comes from experiments using electron diffraction by large water clusters supercooled to 200 K (ref. 34), and from experiments that measure the velocity distribution of evaporating water molecules from a liquid water jet at 210 K (ref. 35). Additionally, recent computational molecular-dynamics studies of the self diffusion of water molecules in the deeply supercooled liquid state also support the view that no thermodynamic instability is required to explain the anomalous behaviour of the transport properties near the proposed temperature singularity[36]—although these simulations use the SPC-E water potential which is known to represent inadequately some aspects of the normal liquid behaviour.

Taken together, the above results, combined with our previous demonstration of a thermodynamic continuity[17], suggest that at the calorimetric glass transition temperature of 136 K (ref. 31) the amorphous solid melts into a deeply supercooled metastable extension of normal liquid water before crystallizing near 160 K. This interpretation does not require the existence of a temperature singularity near 228 K (ref. 2) at low pressure (<0.1 MPa), and is consistent with (but is not proof of) the existence of a second critical point near 220 K and 0.1 GPa (refs 8, 12). Although our ASW diffusivity data provide support for a continuity between ASW and liquid water at low pressure, an unambiguous resolution of the continuity conundrum must await further experiments in the unexplored temperature region from 160 to 240 K. Such experiments will be difficult because of the rapid crystallization of supercooled liquid water below 230 K, and of ASW above 160 K. □

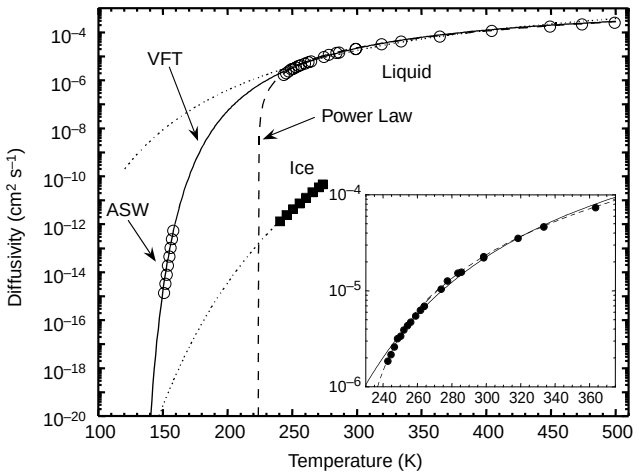

Figure 3 Temperature dependence of diffusivity. Open circles show the ASW diffusivity in the temperature range 150–157 K. Also shown are data for the diffusivity of liquid[24] and supercooled liquid[25,26] water (open circles) and crystalline ice[22,23] (filled squares). The dotted lines are Arrhenius extrapolations of these diffusivities. The solid line labelled VFT is a fit of the liquid/supercooled liquid data and ASW diffusivity data to the Vogel–Fulcher–Tammann (VFT) equation, $D = D_0 e^{-(E/(T-T_0))}$, where $D_0 = 3.06 \times 10^{-3}$ cm^2 s^{-1}, $E = 892$ K and $T_0 = 118$ K are the parameters. The dashed line labelled Power Law is a fit to the high-temperature ($T > 240$ K) liquid/supercooled liquid data to the power-law equation[28], $D = D_0 T^{1/2}(T/T_s - 1)^{\gamma}$, where $D_0 = 8.9 \times 10^{-6}$ cm^2 s^{-1}, $\gamma = 1.75$ and $T_s = 223.4$ K are the parameters. While the power-law and VFT equations fit the high-temperature data reasonably well, the power law is incompatible with the new low-temperature ASW data reported here. Inset, expanded scale view of the high-temperature diffusivity data[24–26] (filled circles) and the VFT (solid line) and power-law (dashed line) fits. Above 250 K, both the VFT and power laws give reasonable fits, but below 250 K the VFT curve misses the data by ~25% and the power law fits the data better.

Received 31 December 1998; accepted 17 February 1999.

1. Mishima, O. & Stanley, H. E. The relationship between liquid, supercooled and glassy water. *Nature* **396,** 328–335 (1998).
2. Speedy, R. J. & Angell, C. A. Isothermal compressibility of supercooled water and evidence for a thermodynamic singularity at −45 °C. *J. Chem. Phys.* **65,** 851–858 (1976).
3. Angell, C. A. in *Water: A Comprehensive Treatise* Vol. 7 (ed. Franks, F.) 1–81 (Plenum, New York, 1982).
4. Angell, C. A. Supercooled water. *Annu. Rev. Phys. Chem.* **34,** 593–630 (1983).
5. Debenedetti, P. G. *Metastable Liquids: Concepts and Principles* (Princeton Univ. Press, 1996).
6. Stanley, H. E. & Teixeira, J. Interpretation of the unusual behavior of H_2O and D_2O at low temperatures: a test of a percolation model. *J. Chem. Phys.* **73,** 3404–3422 (1980).
7. Speedy, R. J. Stability limit conjecture. An interpretation of the properties of water. *J. Chem. Phys.* **86,** 982–991 (1982).
8. Poole, P. H., Sciotino, F., Essman, U. & Stanley, H. E. Phase behaviour of metastable water. *Nature* **360,** 324–328 (1992).
9. Poole, P. H., Sciotino, F., Grande, T., Stanley, H. E. & Angell, C. A. Effect of hydrogen bonds on the thermodynamic behavior of liquid water. *Phys. Rev. Lett.* **73,** 1632–1635 (1994).
10. Borick, S. S., Debenedetti, P. G. & Sastry, S. A lattice model of network forming fluids with orientation-dependent bonding: equilibrium, stability, and implications for the phase behavior of supercooled water. *J. Phys. Chem.* **99,** 3781–3792 (1995).
11. Tanaka, H. A self-consistent phase diagram for supercooled water. *Nature* **380,** 328–330 (1996).
12. Mishima, O. & Stanley, H. E. Decompression-induced melting of ice IV and the liquid-liquid transition in water. *Nature* **392,** 164–168 (1998).
13. Xie, Y., Ludwig, K. F. Jr, Morales, G., Hare, D. E. & Sorensen, C. M. Noncritical behavior of density fluctuations in supercooled water. *Phys. Rev. Lett.* **71,** 2050–2053 (1993).
14. Sceats, M. G. & Rice, S. A. in *Water: A Comprehensive Treatise* Vol. 7 (ed. Franks, F.) 83–214 (Plenum, New York, 1982).
15. Fisher, M. & Devlin, J. Defect activity in amorphous ice from isotopic exchange data: Insight into the glass transition. *J. Phys. Chem.* **99,** 11584–11590 (1995).
16. Speedy, R. J. Evidence for a new phase of water: water II. *J. Phys. Chem.* **96,** 2322–2325 (1992).
17. Speedy, R. J., Debenedetti, P. G., Smith, R. S., Huang, C. & Kay, B. D. The evaporation rate, free energy, and entropy of amorphous water at 150K. *J. Chem. Phys.* **105,** 240–244 (1996).
18. Smith, R. S., Huang, C. & Kay, B. D. Evidence for molecular translational diffusion during the crystallization of amorphous solid water. *J. Phys. Chem. B* **101,** 6123–6126 (1997).
19. Brown, D. E. *et al.* H_2O condensation coefficient and refractive index for vapor-deposited ice from molecular beam and optical interference measurements. *J. Phys. Chem.* **100,** 4988–4995 (1996).
20. Smith, R. S., Huang, C., Wong, E. K. L. & Kay, B. D. Desorption and crystallization kinetics in nanoscale thin films of amorphous water ice. *Surf. Sci. Lett.* **367,** L13–L17 (1996).
21. Smith, R. S., Huang, C., Wong, E. K. L. & Kay, B. D. The molecular volcano: abrupt CCl_4 desorption driven by the crystallization of amorphous solid water. *Phys. Rev. Lett.* **79,** 909–912 (1997).
22. Onsager, L. & Runnels, L. K. Diffusion and relaxation phenomena in ice. *J. Chem. Phys.* **50,** 1089–1103 (1969).
23. Goto, K., Hondoh, T. & Higashi, A. Determination of diffusion coefficients of self-interstitials in ice with a new method of observing climb of dislocations by X-ray topography. *Jpn J. Appl. Phys.* **25,** 351–357 (1986).
24. Weingärtner, H. Self diffusion in liquid water. A reassessment. *Z. Phys. Chem.* **132,** 129–149 (1982).
25. Prielmeier, F. X., Lang, E. W., Speedy, R. J. & Lüdemann, H.-D. The pressure dependence of self diffusion in supercooled light and heavy water. *Ber. Bunsenges. Phys. Chem.* **92,** 1111–1117 (1988).
26. Gillen, K. T., Douglass, D. C. & Hoch, M. J. R. Self-diffusion in liquid water to −31 °C. *J. Chem. Phys.* **57,** 5117–5119 (1972).
27. Angell, C. A. Formation of glasses from liquids and biopolymers. *Science* **267,** 1924–1934 (1995).
28. Prielmeier, F. X., Lang, E. W., Speedy, R. J. & Lüdemann, H.-D. Diffusion in supercooled water to 300 MPa. *Phys. Rev. Lett.* **59,** 1128–1131 (1987).
29. Angell, C. A. Approaching the limits. *Nature* **331,** 206–207 (1988).
30. Handa, Y. P. & Klug, D. D. Heat capacity and glass transition behavior of amorphous ice. *J. Phys. Chem.* **92,** 3323–3325 (1988).
31. Johari, G. P., Hallbrucker, A. & Mayer, E. The glass-liquid transition of hyperquenched water. *Nature* **330,** 552–553 (1987).
32. Johari, G. P. Liquid state of low-density pressure-amorphized ice above its T_g. *J. Phys. Chem. B* **102,** 4711–4714 (1998).
33. Johari, G. P. Water's character from dielectric relaxation above its T_g. *J. Chem. Phys.* **105,** 7079–7082 (1996).
34. Bartell, L. S. & Huang, J. Supercooling of water below the anomalous range near 226 K. *J. Phys. Chem.* **98,** 7455–7457 (1994).
35. Faubel, M., Schlemmer, S. & Toennies, J. P. A molecular beam study of the evaporation of water from a liquid jet. *Z. Phys. D* **10,** 269–277 (1988).
36. Gallo, P., Sciortino, F., Tartaglia, P. & Chen, S.-H. Slow dynamics of water moelcules in supercooled states. *Phys. Rev. Lett.* **76,** 2730–2733 (1996).
37. Stevenson, K. P., Kimmel, G. A., Dohnálek, Z., Smith, R. S. & Kay, B. D. Controlling the morphology of amorphous solid water. *Science* **283,** 1505–1507 (1999).

Acknowledgements. We thank C. A. Angell, H. E. Stanley, R. J. Speedy, P. Debenedetti, E. Mayer, S. Sastry, P. Poole, F. Sciortino, F. Starr, H. D. Lüdemann and A. Geiger for discussions. This work was supported by the US Department of Energy, Office of Basic Energy Sciences, Chemical Sciences Division. Pacific Northwest National Laboratory is operated for the US Department of Energy by Battelle.

Correspondence and requests for materials should be addressed to B.D.K. (e-mail: bd_kay@pnl.gov).